Earth Planet. Sci. Lett. 629 (2024) 118618

Contents lists available at ScienceDirect

Earth and Planetary Science Letters

journal homepage: www.elsevier.com/locate/epsl

Composition of Earth's initial atmosphere and fate of accreted volatiles set by core formation and magma ocean redox evolution

Jesse T. Gu [a,*], Bo Peng [b], Xuan Ji [c], Jisheng Zhang [d], Hong Yang [e], Susana Hoyos [f], Marc M. Hirschmann [g], Edwin S. Kite [c], Rebecca A. Fischer [a]

[a] *Department of Earth and Planetary Sciences, Harvard University, Cambridge, MA, United States*
[b] *Department of Astronomy and Astrophysics, University of Toronto, Toronto, ON, Canada*
[c] *Department of the Geophysical Sciences, University of Chicago, Chicago, IL, United States*
[d] *Department of Astronomy and Astrophysics, University of Chicago, Chicago, IL, United States*
[e] *Department of Earth and Planetary Sciences, Stanford University, Stanford, CA, United States*
[f] *Department of Earth, Atmospheric, and Planetary Sciences, Massachusetts Institute of Technology, Cambridge, MA, United States*
[g] *Department of Earth and Environmental Sciences, University of Minnesota, Minneapolis, MN, United States*

ARTICLE INFO

Keywords:
Core formation
Magma ocean
Volatiles
Early atmosphere
Accretion

ABSTRACT

The origins of volatile depletion in the Bulk Silicate Earth (BSE) remain controversial due to the numerous processes during accretion and differentiation that can alter volatile abundances. Here, we integrate realistic impact histories from *N*-body simulations to determine the distribution of H, C, and N between Earth's core, mantle, and atmosphere, including loss to space, during the giant impact stage of accretion. Estimates of the BSE's volatile abundances can be matched if accreting materials were depleted ~1–2 orders of magnitude relative to CI chondrite volatile abundances, indicating early volatile loss on planetesimals and embryos prior to terrestrial accretion. We find the proto-Earth's atmosphere to be dominated by CO (>97%), which leads to the preferential erosion of C relative to H and N by subsequent impacts. Erosion can remove significant C (~18–45% of accreted C), and potentially substantial N as well (~12–23%), if N is not extremely siderophile at high pressures and temperatures. Out of the accreted volatiles, the majority are sequestered in the core, which is the largest reservoir of H (~57–75%), C (~54%–98%), and N (~69%–99.9%) in the bulk Earth after accretion. Our results show that the BSE's volatile depletion relative to chondrites is dominated by loss on precursor bodies (>92%), followed by core formation (~77–99% of remaining <8%), while atmosphere erosion accounts for the rest. Formation scenarios that source more material from the outer Solar System, such as Classical and Grand Tack, result in Earth analogs that have higher total volatile concentrations, lower proportions of volatiles stored in Earth analog cores, and have lost a larger fraction of their accreted C due to atmosphere erosion. The BSE's superchondritic C/N ratio can be matched or exceeded, even if Earth's building blocks have CI chondritic C/N, if N is more strongly siderophile at high pressures and temperatures. If N does not become sufficiently siderophile at high pressures and temperatures, however, Earth's building blocks must have accreted with superchondritic C/N ratios.

1. Introduction

Volatile elements, such as H, C, and N, are essential for Earth's habitability. The distribution of these elements during Earth's formation sets their availability at the surface at the beginning of Earth's evolution. Therefore, understanding the processes that affect the abundances of volatile elements at Earth's surface during its formation are crucial to understanding how Earth came to be habitable. The Bulk Silicate Earth (BSE) is depleted in volatile elements relative to chondrites (Broadley et al., 2022; Halliday, 2013; Marty and Zimmermann, 1999), but the source of this volatile depletion remains unclear, as multiple processes can alter volatile abundances during Earth's formation. Prior to the giant impact stage of Earth's accretion, condensation from the protoplanetary disk and differentiation and growth of planetesimals and embryos shape the volatile inventories of Earth's building blocks (Hirschmann et al., 2021; Li et al., 2021; Lichtenberg et al., 2019;

* Corresponding author.
E-mail address: jessegu@g.harvard.edu (J.T. Gu).

https://doi.org/10.1016/j.epsl.2024.118618
Received 14 July 2023; Received in revised form 2 February 2024; Accepted 7 February 2024
Available online 14 February 2024

Newcombe et al., 2023; Young et al., 2023). Subsequently, core formation, magma ocean degassing, and impact erosion by planetesimal and embryo impacts could all have altered the abundances of volatiles in the silicate and surface inventories of rocky planets (Abe and Matsui, 1986; Chen and Jacobson, 2022; Genda and Abe, 2005; Hirschmann, 2016; Sossi et al., 2022; Tucker and Mukhopadhyay, 2014). Even in some pebble accretion scenarios, Earth is formed from two large embryos that experienced their own volatile histories before colliding with one another (Johansen et al., 2021).

Estimates of the BSE's H, C, and N budgets indicate that these elements are depleted by several orders of magnitude relative to carbonaceous chondrites (Hirschmann, 2018; Marty, 2012; Marty et al., 2020; Marty and Zimmermann, 1999). In particular, the BSE is characteristically more depleted in N relative to H and C. It is possible that Earth formed from planetesimals and embryos that already had superchondritic C/N ratios (Grewal and Asimow, 2023; Li et al., 2023). The BSE's C/N could also have been modified by core formation, magma ocean outgassing, and/or impact erosion (Bergin et al., 2015; Hirschmann, 2016). The effects of core formation and magma ocean outgassing on the distribution of volatile elements during Earth's accretion remains an open question, however, as previous models neglected the effects of evolving conditions throughout Earth's formation (Chen and Jacobson, 2022; Sakuraba et al., 2021). For example, pressures and temperatures of core formation are expected to increase and magma oceans are expected to become more oxidized throughout accretion (Rubie et al., 2015). The core may be Earth's largest reservoir of volatiles (Fischer et al., 2020; Okuchi, 1997), so quantifying its volatile budget is key to understanding the effects of core formation on Earth's volatile element ratios. In addition, the redox evolution of magma oceans, which is set by core-forming metal, determines the speciation of H and C in the overlying atmosphere (Deng et al., 2020; Gaillard et al., 2022; Hirschmann, 2012; Zhang et al., 2017). Various atmospheric species have unique solubilities in silicate liquids, resulting in different distributions of volatile elements between magma oceans and atmospheres (Bower et al., 2022; Hirschmann, 2012). As a result, the susceptibility of each volatile element to erosion by subsequent impacts is linked to its distribution between core, mantle, and atmosphere, which is determined by the conditions of core formation and magma ocean redox states.

Recent geochemical models of core formation include evolving pressures, temperatures, and oxygen fugacities (fO_2) of metal–silicate equilibration throughout accretion (e.g., Fischer et al., 2017; Gu et al., 2023; Rubie et al., 2015), but incorporating volatile elements remains a challenge because these models do not include the overlying atmosphere. In addition, the timing and quantity of volatile delivery may be heterogeneous, resulting in selective sequestration of volatile elements in the core under certain conditions (Schönbächler et al., 2010; Sossi et al., 2022). The degree to which impact erosion can modify volatile abundances is a result of the proportion of volatile elements in the atmosphere available to be eroded. Estimates of the initial volatile concentrations in accreting material and resulting core concentrations therefore may be biased (Blanchard et al., 2022; Fischer et al., 2020; Jackson et al., 2021). Understanding the timing of volatile accretion and the distribution of volatile elements between core, mantle, atmosphere, and loss to space will not only help to constrain the composition of the Earth's core, but also the extent of volatile depletion on Earth's precursor materials.

Here, we model planetary growth, core formation, magma ocean degassing, and impact erosion during the giant impact stage of Earth's accretion (Fig. 1). Our accretion histories are based on *N*-body simulations, combined with a core formation model that incorporates the effects of evolving pressures and temperatures on the partitioning of light elements into Earth's core. This allows fO_2 to evolve over the course of accretion, both at the metal–silicate interface, and throughout the magma ocean, linking the speciation and solubility of each volatile element in the atmosphere to the interior (Armstrong et al., 2019; Deng et al., 2020; Kuwahara et al., 2023). We focus on the distribution of H, C, and N within the proto-Earth to constrain the extents to which core formation and impact erosion contributed to the BSE's present-day volatile depletion, therefore setting bounds on the initial volatile inventory of Earth's building blocks.

2. Methods

2.1. Initial conditions

Accretion histories of Earth analogs are taken from 433 published *N*-body simulations spanning Classical, Annulus, Grand Tack, and Early Instability models of Solar System formation (Clement et al., 2021;

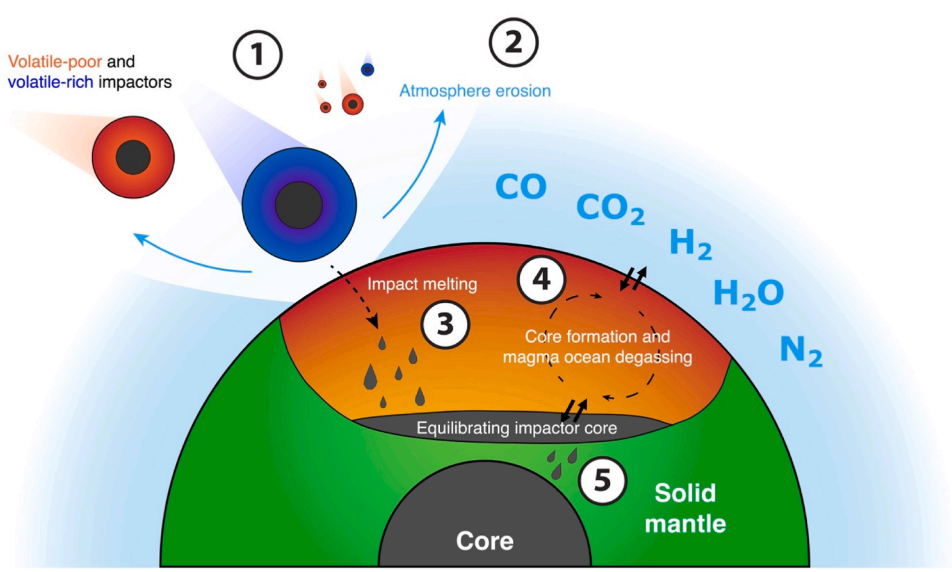

Fig. 1. Schematic representation of model steps for each impactor. 1) Volatile elements are assigned to impactors based on their initial semi-major axes, which are taken from *N*-body simulations. 2) Each impactor erodes a portion of the existing atmosphere and 3) melts a fraction of the proto-Earth's mantle. 4) Volatile elements are distributed between a portion of the impactor's core, the molten mantle, and the remaining atmosphere based on metal–silicate partitioning coefficients, solubilities of atmosphere species in the magma, and the fO_2 at the surface of the magma ocean. 5) The equilibrated core material sinks and merges with the proto-Earth's core.

Jacobson and Morbidelli, 2014; O'Brien et al., 2006; Raymond et al., 2009; Raymond and Izidoro, 2017). Earth analogs are defined as the planet at the end of each simulation closest to 1 Earth mass (in the range 0.8–1.25 Earth masses) and 1 AU (in the range 0.8–1.2 AU), resulting in a total of 85 Earth analogs (Gu et al., 2023). All bodies are assigned initial compositions based on refractory elemental abundances in CI chondrites (Palme and O'Neill, 2014). Volatile abundances and bulk fO_2 of accreting bodies are prescribed based on their original semi-major axes (Fischer et al., 2017; Rubie et al., 2015). Following previous models, we use different values of fixed fO_2 for bodies from within (IW–2.75) and beyond (IW–1.50) 2 AU, with inner Solar System bodies being more reduced (fO_2 expressed in log units relative to the iron–wüstite buffer). The fO_2 values and fO_2 cutoff at 2 AU are chosen to match Earth's mantle FeO, as well as be consistent with Mars' accretion (Brennan et al., 2022; Gu et al., 2023). Likewise, volatile concentrations are assigned in CI chondritic proportions (Vacher et al., 2020; Wasson and Kallemeyn, 1988), but are depleted by a constant factor based on each body's initial semi-major axis. The model values for each of these parameters are given in Table 1. We assume that material originating from beyond 2 AU is ten times more enriched in volatile elements than material originating from within 2 AU because carbonaceous chondrites have about an order of magnitude more H, C, and N than enstatite chondrites (Table 1 of Sakuraba et al., 2021 and references therein). The sensitivity of our model to these parameters (location of fO_2 cutoff, fO_2 values, chondrite type, and volatile abundances) is explored in Supplementary Text S5. Volatile elements are initially distributed between cores and mantles of planetesimals and embryos (Supplementary Text S1). We do not explicitly model volatile loss on these bodies. Therefore, assigned initial volatile abundances represent bulk volatile abundances at the time of their accretion onto the proto-Earth.

2.2. Atmosphere erosion

The fraction of existing atmosphere eroded by each impact is determined based on the properties of the impactor and atmosphere at the time of the impact. We adopt separate prescriptions for planetesimal and embryo impacts, taking into account the size distribution of planetesimals and differences in erosional properties of aerial bursts and giant, cratering, and fragmenting impacts (Kegerreis et al., 2020; Schlichting et al., 2015; Shuvalov, 2009; Shuvalov et al., 2014; Sinclair and Wyatt, 2022).

Planetesimals in *N*-body simulations represent conglomerations of smaller bodies that are assumed to impact simultaneously. A power law size distribution with a differential power law index of $q = 2$ is used to describe the impactor size distribution for each planetesimal such that $\frac{dN}{dD} \propto D^{-q}$, where N is the number of impactors smaller than diameter D (Fig. S1) (Sakuraba et al., 2021). Impactors have minimum (D_{min}) and maximum (D_{max}) diameters of 1 and 1000 km, respectively. Assuming an impactor density of $\rho_i = 3.3$ g/cm^3 and that the mass of a planetesimal scales with its diameter as $m_i = \frac{\pi \rho_i D^3}{6}$, the size distribution of planetesimals is converted to a mass distribution. A random sample equivalent to a specified total planetesimal mass, M_{ptsml}, is generated from this distribution:

$$N = \frac{12 M_{ptsml}}{\pi \rho_i} \left(D_{max} D_{min} (D_{max} + D_{min}) \right)^{-1} \tag{1}$$

Atmosphere loss from planetesimal accretion can be induced by cratering if the impactor reaches the surface intact. Otherwise, impactors may fragment or form aerial bursts before reaching the surface. We adopt the prescription of Shuvalov et al. (2014), as modified by Sinclair and Wyatt (2022), to describe fragmenting impacts and aerial bursts and that of Shuvalov (2009) for cratering impacts (Fig. S2). We also include the polar cap limit from Schlichting et al. (2015), which limits the atmosphere loss due to a single impact. Further details of these methods are described in Supplementary Text S2.

Giant impacts associated with embryo collisions erode existing atmospheres by ejecting mass near the impact site, but also by causing a shock wave to propagate through the planet, resulting in global ground motion (Genda and Abe, 2005; Schlichting et al., 2015). Embryo masses are taken directly from *N*-body simulations. We apply the scaling law of Kegerreis et al. (2020) to describe the fraction of atmosphere lost (X_{loss}) for each embryo impact, defined as impactors with masses >0.01 Earth masses:

$$X_{loss} = 0.64 \left[\left(\frac{v_i}{v_{esc}} \right)^2 \left(\frac{M_i}{M_i + M_p} \right)^{\frac{1}{2}} \left(\frac{\rho_i}{\rho_p} \right)^{\frac{1}{2}} f_M(b) \right]^{0.65} \tag{2}$$

where $\frac{v_i}{v_{esc}}$ is the impact velocity normalized to the escape velocity, $\frac{M_i}{M_i + M_p}$ is the impactor:total mass ratio, and $\frac{\rho_i}{\rho_p}$ is the impactor:target density ratio. $f_M(b)$ is a fractional interacting mass (Supplementary Text S2). We do not incorporate atmospheric loss induced by thermal expansion of the atmosphere since thermal loss is inefficient for high mean molecular mass envelopes (Biersteker and Schlichting, 2021).

2.3. Volatile distribution between metal, silicate, and atmosphere

Following each impact, it is assumed that a fraction of the impactor's core, the molten portion of the target's mantle, and the entire remaining atmosphere is equilibrated. The fraction of the mantle that is melted by the impact (k_{mantle}) is determined from existing scaling laws (Abramov et al., 2012; Nakajima et al., 2021). For impactors >0.01 Earth masses (embryos), the impactor and target masses, impact velocity, and impact angle of each collision were extracted from the outputs of each *N*-body simulation and used in the melt-scaling law from Nakajima et al. (2021), which parameterizes outputs from hydrodynamic simulations to determine the volume and geometry of melting in the target's mantle. Impact angles were rounded to the nearest available angle (0°, 30°, 45°, 60°, 90°) with surface entropy set to 1100 J/K/kg, corresponding to surface temperatures of ~300 K. Only a fraction of impacting embryo cores participates in equilibration ($k_{core\_emb} = 0.3$), since cores of larger bodies are more likely to directly merge with the proto-Earth's core (Marchi et al., 2018; Rubie et al., 2015). Planetesimal cores, on the other hand, are considered to completely equilibrate (Kendall and Melosh, 2016). These planetesimals were equilibrated with a portion of the mantle equal to five times the impactor's mantle mass, consistent with estimates of melting using the average impact velocity and averaged over all impact angles (Abramov et al., 2012; Gu et al., 2023). Planetesimal cores are assumed to remain in the mantle and are then re-equilibrated during the next embryo impact (Fleck et al., 2018).

Major elements Fe, Si, Ni, and O are partitioned between the fraction of equilibrating impactor core and the molten portion of the mantle, whereas Mg, Ca, and Al are assumed to be perfectly lithophile. The partitioning parameterization used for each element can be found in Table S1. Equilibration pressures evolve along a predetermined pressure

Table 1
Volatile concentrations (ppmw) in the BSE, CI chondrites, and prescribed to accreting bodies. Inner and outer refer to bodies originating from within and beyond 2 AU, respectively. The effects of varying volatile concentrations, H:C:N ratios, and inner:outer Solar System abundance ratios are explored in Supplementary Text S5 and the Supplementary Data.

	H	C	N
BSE[1]	33–750	42–730	0.83–2.5
CI chondrite[2]	6000	32,000	1500
Inner (2% CI)	120	640	30
Outer (20% CI)	1200	6400	300

[1] BSE constraints are from Marty (2012), Hirschmann (2018), and Marty et al. (2020).
[2] CI chondrite values are from Wasson and Kallemeyn (1988) and Vacher et al. (2020).

history, corresponding to the evolving average pressure at the base of magma oceans, which is derived from embryo impacts averaged over many *N*-body simulations coupled with a melt-scaling law (Fig. S3) (Gu et al., 2023; Nakajima et al., 2021). This is done to simplify pressure calculations, remove the dependence of pressure on initial embryo masses in different simulations, and avoid the need for an ad hoc parameter describing the fractional depth at which metal–silicate equilibration occurs. At each equilibration pressure, the equilibration temperature is set to that of the chondritic liquidus (Andrault et al., 2011), and temperature is extrapolated upwards through the magma ocean along the liquid adiabat (Thomas and Asimow, 2013). Partitioning of major elements sets the fO_2 of the core–mantle boundary relative to the iron–wüstite buffer, approximated (assuming ideal mixing) as:

$$\Delta IW = 2log\left(\frac{X_{FeO}}{X_{Fe}}\right) \tag{3}$$

where X_{FeO} is the mole fraction of FeO in the mantle and X_{Fe} is the mole fraction of Fe in the core. Assuming a constant Fe^{3+}/Fe_{tot} throughout the magma ocean due to vigorous convection, fO_2 is extrapolated upwards along the liquid adiabat (Thomas and Asimow, 2013) of the magma ocean to determine the fO_2 at the magma ocean–atmosphere interface (Deng et al., 2020; Hirschmann, 2021, 2022). Magma ocean fO_2 evolves with increasing Fe^{3+}/Fe_{tot} as Earth analogs grow and magma ocean depths increase (Deng et al., 2020). Details of these calculations are discussed in Supplementary Text S3. We also test a scenario, based on recent experimental results from Kuwahara et al. (2023), where magma oceans are more oxidized with Fe^{3+}/Fe_{tot} of ∼0.3–0.4 in Supplementary Text S4. However, oxidized magma oceans are inconsistent with the present-day oxidation state of Earth's mantle (Section 4.1.) (Hirschmann, 2023). Vertically linking fO_2 from the equilibrating impactor core to the atmosphere allows for the self-consistent calculation of volatile distributions of between metal, silicate, and atmosphere.

Volatile elements are partitioned between the equilibrating impactor core, molten mantle, and remaining atmosphere by mass balance, such that:

$$M_i^{tot} = X_i^{met}M^{met} + X_i^{sil}M^{sil} + \sum \frac{4\pi R^2 m_i^{atm}}{g\mu r_i}P_i \tag{4}$$

where M_i^{tot} is the total mass of volatile element *i*, P_i is the partial pressure of each species of element *i* in the atmosphere, R is the current radius of the proto-Earth at the time of the impact, g is its associated gravitational acceleration, μ is the mean molecular mass of the atmosphere, m_i^{atm} is the molecular mass of each species of element *i* in the atmosphere, and r_i is the mass ratio of the volatile species to the element of interest (e.g., $m_{CO}/m_C = 28/12$) (Bower et al., 2019; Sakuraba et al., 2021). X_i^{met} and X_i^{sil} are the concentrations of element *i* in the equilibrating metal and silicate reservoirs, respectively, which have total masses M^{met} and M^{sil}. The summation for the atmospheric term in Eq. (4) is for H and C, which can exist as Multiple species (H_2O or H_2, and CO_2 or CO, respectively), whereas N_2 is assumed to be the only species for N. The mass balance can be solved given a metal–silicate partition coefficient ($D_i = \frac{X_i^{met}}{X_i^{sil}}$), a solubility law relating the partial pressure of each species in the atmosphere to its concentration in the silicate melt, and the relative proportions of H_2O/H_2 or CO_2/CO in the atmosphere. Metal–silicate partitioning parameterizations (Fig. S4) (Blanchard et al., 2022; Jackson et al., 2021; Shi et al., 2022; Tagawa et al., 2021) and solubility laws (Dasgupta et al., 2022; Lichtenberg et al., 2021) are described in Supplementary Text S3. We do not account for the interactions between light elements in the metal, as the magnitudes of these interactions at high pressures and temperatures are uncertain and likely to be small for these X_i^{met}. We use two parameterizations for the metal–silicate partitioning of N to bound its partitioning behavior, where "J21" refers to the more siderophile parameterization of Jackson et al. (2021) and "S22" refers to the less siderophile parameterization of Shi et al. (2022). For C, we use the parameterization from Blanchard et al. (2022), which predicts a higher siderophility of C at high pressures and temperatures than the parameterization from Fischer et al. (2020). C being more siderophile diminishes its abundance in the mantle and atmosphere, so that the amount of C lost to space in our model represents a lower bound (Supplementary Data). At the surface of the magma ocean, chemical equilibrium distributes H and C budgets into H_2/H_2O and CO/CO_2 given the surface fO_2 and temperature. The two reactions involved are:

$$H_2O \leftrightarrow H_2 + \frac{1}{2}O_2 \tag{5}$$

$$CO_2 \leftrightarrow CO + \frac{1}{2}O_2 \tag{6}$$

The equilibrium constants for these two reactions are computed following the methods of Robie and Hemingway (1995), with the thermodynamic quantities from Linstorm (1998).

We define a set of plausible reference parameters that reproduce mantle FeO and trace element compositions (Gu et al., 2023; McDonough and Sun, 1995; Palme and O'Neill, 2014) to constrain $k_{core\_emb} = 0.3$, inner $fO_2 = $ IW–2.75, outer $fO_2 = $ IW–1.5, fO_2 cutoff = 2 AU, $P_{max} = 60$ GPa, and k_{mantle} set by melt-scaling laws, which are the parameters to which core formation models are most sensitive (Fischer et al., 2017). The sensitivity of our model to individual parameters is discussed in Supplementary Text S5. Initial volatile concentrations are then varied to provide reasonable matches to estimates for the BSE's volatile concentrations. In our reference case, inner Solar System materials have 2% and outer Solar System materials have 20% CI chondrite concentrations of H, C, and N (Table 1). Our prescription of equilibration corresponds to magma oceans that crystallize between impacts such that we can employ scaling laws for mantle melting and atmosphere erosion that assume solid surfaces. This is because the timescale of magma ocean crystallization for atmospheres formed by our model are fleeting relative to the time between impacts (Gu et al., 2023; Lichtenberg et al., 2021; Nikolaou et al., 2019). We assume that equilibration between core, mantle, and atmosphere is shorter than the magma ocean crystallization timescale (Salvador and Samuel, 2023; Thomas et al., 2023) and that the distribution of volatile elements between the mantle and atmosphere is not altered due to magma ocean crystallization between impacts. We run additional models to test the effects of volatile outgassing between impacts in Section 4.2. Our model links realistic impact histories to the self-consistent distribution of volatile elements between the proto-Earth's core, mantle, atmosphere, and loss to space.

3. Results

3.1. Fate of accreted volatiles

Earth analog mantles naturally become progressively oxidized over the course of accretion due to the incorporation of more Si in the core at higher *P–T* (with more corresponding oxidation of Fe) and the tendency of Earth analogs to accrete more oxidized bodies from beyond 2 AU at later times (O'Brien et al., 2006), resulting in higher Fe_{tot} and Fe^{3+}/Fe_{tot} (Fig. 2) (Rubie et al., 2011). Oxidation of the mantle, combined with the increasing depths of magma oceans, generates increasingly oxidized surface fO_2 values that evolve from ∼IW–3 to ∼IW–1 (Fig. 3a) (Deng et al., 2020; Hirschmann, 2022, 2021). These fO_2 values correspond to Fe^{3+}/Fe_{tot} values of ∼0.01 and ∼0.05 (Fig. 2b). Despite becoming more oxidized relative to equilibrium with Fe alloy, surface fO_2 values remain below the iron–wüstite buffer. We note that using the data of Sossi et al. (2020) to determine fO_2 would result in more oxidized surface fO_2 by ∼1 log unit. We also consider a more extreme oxidized case in Supplementary Text S4, where magma oceans have high Fe^{3+}/Fe_{tot} (Kuwahara et al., 2023), but note that this case is inconsistent with the mantle's redox budget and long-term evolution (Hirschmann, 2023).

The abundance of H, C, and N stored in the core and lost to space is a

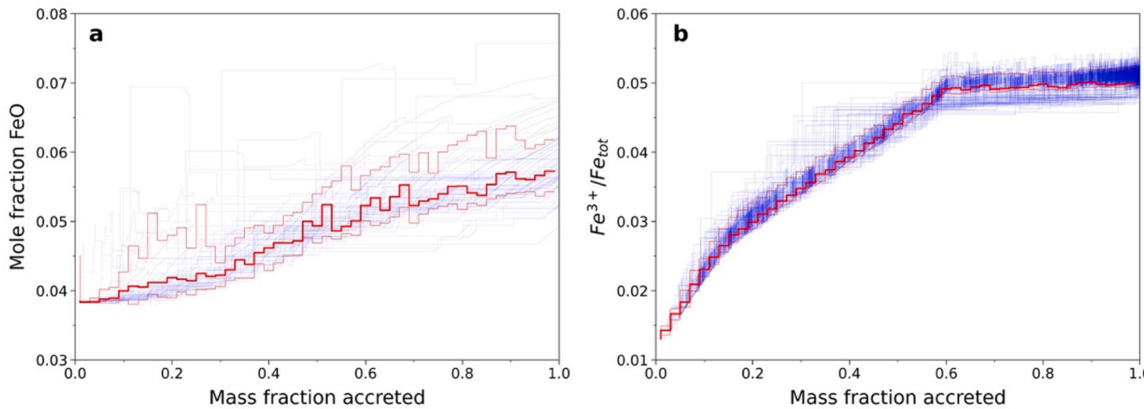

Fig. 2. (a) Mantle FeO contents and (b) Fe^{3+}/Fe_{tot} ratios in Earth analogs throughout accretion. Bold red lines are the medians and semi-bold red lines are the 10th and 90th percentiles of all Earth analogs. Thin blue lines correspond to the evolution of individual Earth analogs. Bulk fO_2 of accreting bodies are adjusted so that Earth analogs match Earth's ∼8 wt% FeO, on average, at the end of accretion. FeO contents in Earth analog mantles progressively increase due to core formation. Higher FeO and deeper magma oceans promote oxidation of the mantle.

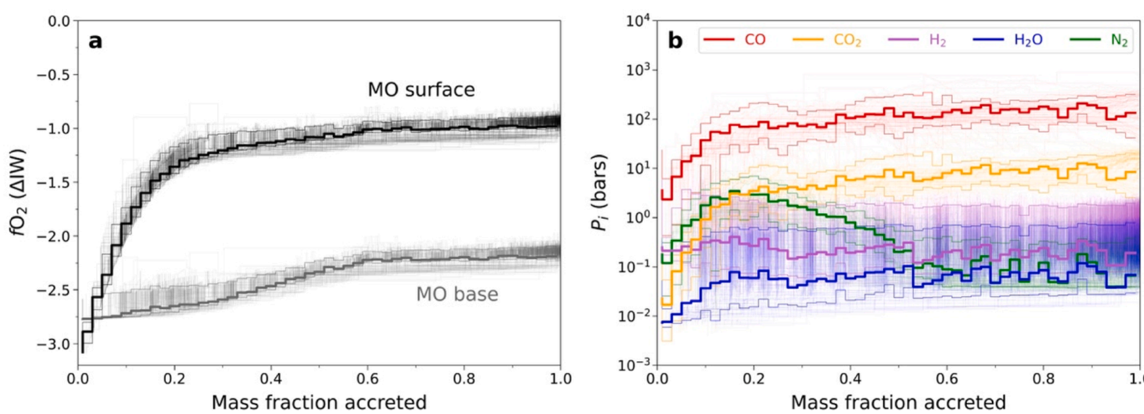

Fig. 3. Evolution of (a) fO_2 at the base and surface of the magma ocean and (b) atmosphere composition of Earth analogs. Bold lines are medians and semi-bold lines are 10th and 90th percentiles of all Earth analogs. Thin lines are evolutions of individual Earth analogs. Magma oceans remain below the iron–wüstite buffer, resulting in CO-dominated atmospheres throughout accretion.

function of both their solubilities and their siderophilities at the conditions of core formation. All three elements are predicted to be siderophile, so most of each ends up in the core, with the core making up ∼57–75% and ∼43–75% of accreted H and C, respectively (Fig. 4). These bounds are taken from the smallest 10th percentile and the largest 90th percentile of the distributions of Earth analogs. Storage of N in Earth analog cores is governed by its metal–silicate partition coefficient, which remains uncertain above ∼25 GPa, but can account for ∼55–98% of accreted N (Jackson et al., 2021; Shi et al., 2022). If N is siderophile enough at high pressures and temperatures, core formation could elevate the BSE's C/N ratio relative to its chondritic precursors such that the modeled C/N ratio matches or exceeds the BSE's observed superchondritic C/N ratio (Fig. 5). The exact C/N ratio in this scenario depends on the solubility of N in magma oceans (Fig. S10). However, if N is not as siderophile at high pressures and temperatures, our model fails to reproduce the BSE's superchondritic C/N.

On the other hand, the availability of each element to be lost by atmospheric erosion depends on their solubilities, where H is more soluble than N and C. The high solubility of H, combined with the reduced surfaces of magma oceans, results in CO-dominated atmospheres throughout accretion, with C making up >97% of atmosphere species (Fig. 3b) (Bower et al., 2022; Sossi et al., 2020). Because of this, C is preferentially eroded in subsequent impacts, with ∼18–45% accreted C lost due to atmosphere erosion (Fig. 4). N, on the other hand, can only be eroded to a significant degree (∼12–33%) if it is not strongly siderophile at high pressures and temperatures (Fig. 4). The distribution of volatiles and the abundances of volatile elements that end up in Earth analogs are slightly dependent on simulation type (Figs. 4 and 5). Earth analogs comprised of more material originating from beyond 2 AU, such as those from Classical and Grand Tack simulations, have higher total volatile concentrations, but are more oxidized and so have lower fractions of accreted volatiles in their cores and experience more volatile loss due to atmosphere erosion.

3.2. Origin of the BSE's volatile depletion

Matching estimates for the BSE's H and C contents at the end of accretion, including surface reservoirs (Hirschmann, 2018; Marty, 2012; Marty et al., 2020), requires initial building blocks that are volatile-depleted relative to CI chondrites by ∼1–2 orders of magnitude, on average. If inner Solar System materials have 2% and outer Solar System materials have 20% CI chondrite values (Table 1), the BSE's H and C concentrations can be matched, on average, using inner Solar System materials with ∼0.7–5% CI chondrite concentrations (Fig. S7). This range corresponds to Earth analogs that are made of building blocks, including those originating from beyond 2 AU, containing 0.9%–7.8% CI chondrite concentrations, on average. This means that despite Earth's core being a major reservoir of H, C, and N, and despite significant C, and potentially N loss due to atmosphere erosion, >92% of the BSE's depletion relative to chondrites must have occurred prior to

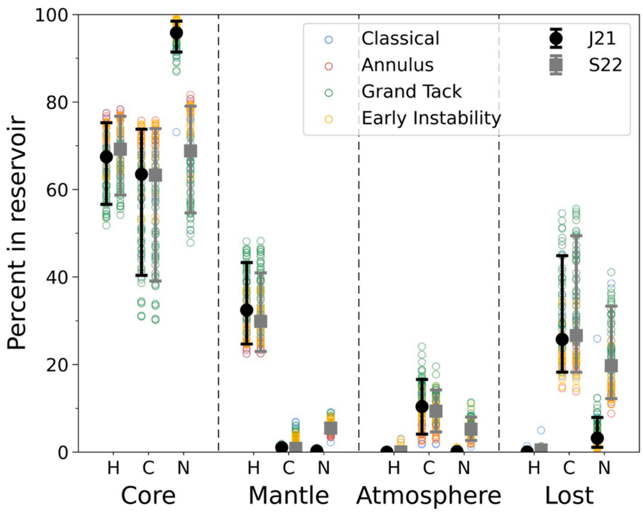

Fig. 4. Distribution of H, C, and N between core, mantle, atmosphere, and loss to space at the end of accretion before magma ocean crystallization. "J21" and "S22" refer to metal–silicate partitioning parameterizations of N from Jackson et al. (2021) and Shi et al. (2022), respectively. Open symbols represent individual Earth analogs and solid black symbols are medians with error bars corresponding to 10th and 90th percentiles of all Earth analogs. The majority of Earth's present-day H, C, and N lies in the core. Atmosphere erosion preferentially erodes C, but can also remove significant N if N is less siderophile.

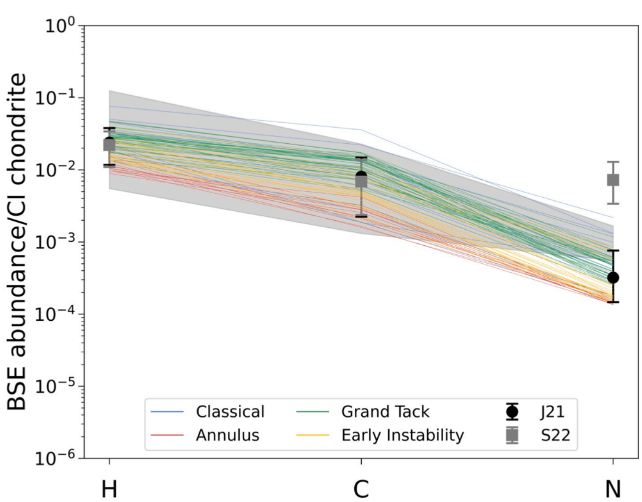

Fig. 5. Abundances of volatile elements in the mantle and atmosphere relative to CI chondrites at the end of accretion. "J21" and "S22" refer to metal–silicate partitioning parameterizations of N from Jackson et al. (2021) and Shi et al. (2022), respectively. The shaded gray region represents estimated bulk Earth abundances (Hirschmann, 2018; Marty, 2012; Marty et al., 2020); lines represent individual Earth analogs from the "J21" scenario. Symbols are medians with error bars corresponding to 10th and 90th percentiles of all Earth analogs. Core formation alone could account for Earth's superchondritic C/N ratio if N becomes siderophile enough at high pressures and temperatures.

accretion onto Earth (Hirschmann et al., 2021; Li et al., 2021; Newcombe et al., 2023). Core formation would make up ~99%, ~78%, and ~77–99% of the remaining <8% depletion in H, C, and N relative to Earth's building blocks with the rest being lost due to atmosphere erosion. Even though atmosphere erosion would be insignificant in setting the BSE's volatile depletion relative to chondrites, it can still erode significant portions of accreted C and N, and therefore, still be important in setting the BSE's C/N ratio.

The estimated average abundances of volatiles in Earth's building blocks are not affected by our assumption of the inner-to-outer Solar System ratio of volatile abundances. If we take an extreme case and assume the inner Solar System is completely dry, our model still reproduces the high C/N ratio of the BSE, on average (Supplementary Text S5). In this scenario, volatiles are delivered based on the timing and quantity of outer Solar System material accreted in each simulation, increasing the spread in final H, C, and N abundances of Earth analogs. Matching Earth's H and C abundances still requires initial building blocks to be depleted by ~1–2 orders of magnitude relative to CI chondrites, on average. Even though the timing and quantity of volatile delivery varies between simulations, core formation always elevates the BSE's C/N ratio relative to its chondritic precursors, challenging the delivery of volatiles solely during the late veneer (e.g., Albarède, 2009). In addition, regardless of the assumed inner-to-outer Solar System ratio of volatiles, atmospheres remain dominated by CO, leading to the preferential loss of C due to atmospheric erosion.

3.3. *Core composition*

The core is generally the largest reservoir of accreted volatiles. When only considering the bulk volatile concentrations remaining in Earth analogs, the core comprises ~57–75%, ~54%–98%, and ~69%–99.9% of the bulk planet's H, C, and N, respectively. These core concentrations are associated with 0.05–0.09 wt% H, 0.25–0.47 wt% C, and 0.01–0.03 wt% N in Earth analog cores. Allowing initial inner Solar System volatile concentrations to vary within the ranges allowed to match estimates of BSE volatile contents (0.7–5%) corresponds to H, C, and N concentrations in Earth analog cores of 0.02–0.24 wt%, 0.08–1.14 wt%, and 0.01–0.08 wt%, respectively. The upper limits of H and C concentrations in the core can account for ~50% of the core's density deficit, but using intermediate values results in H and C accounting for only ~15% of the core's density deficit (Li et al., 2019). Therefore, other light elements, such as Si, O, and S, likely account for the majority of the core's light element budget and density deficit (Fischer et al., 2017) unless there are mechanisms other than core formation that can store light elements in the core (e.g., Young et al., 2023).

Even though our core compositions are affected by averaging over simulation types, our overall model results regarding the distribution of volatile elements during accretion remain robust. H, C, and N abundances in the core vary by <1 mol% throughout accretion, whereas Si and O increase with increasing pressure and temperature as the planet grows based on their metal–silicate partitioning behaviors (Fig. 6). Our reference model yields core concentrations of $2.4^{+0.6}_{-0.5}$ wt% Si and $0.6^{+0.2}_{-0.1}$ wt% O. These abundances are relatively low compared to the ~5–10% concentration of light elements required to match the core's density deficit. However, Si and O are much more sensitive than H, C, and N to the pressure, temperature, and fO_2 of metal–silicate equilibration (Fischer et al., 2017; Gu et al., 2023). We also do not include the mutual interactions of Si and O in the metal (Fischer et al., 2015). Since we are averaging pressures of equilibration and the bulk fO_2 of accreting bodies over different simulation types, the core concentrations of Si and O could vary significantly if these variables are treated independently for each simulation type. For example, simulations that source more material from the outer Solar System would require more initial bodies to be more reduced, which would promote the incorporation of Si in the core. In these simulations, decreasing the inner fO_2 to IW–3.5 increases Si concentrations in the core to $5.4^{+4.7}_{-1.6}$ wt%, but does not significantly affect volatile element concentrations in the core (Supplementary Data), so there are model conditions that can account for whatever portion of the core's density deficit is not explained by H, C, and N through incorporation of other light elements in the core. This initial inner fO_2 is consistent with the mantle's FeO content in some Grand Tack and Classical simulations which source relatively larger fractions of material from beyond 2 AU (Fischer et al., 2017; Gu et al., 2023; Rubie et al., 2015).

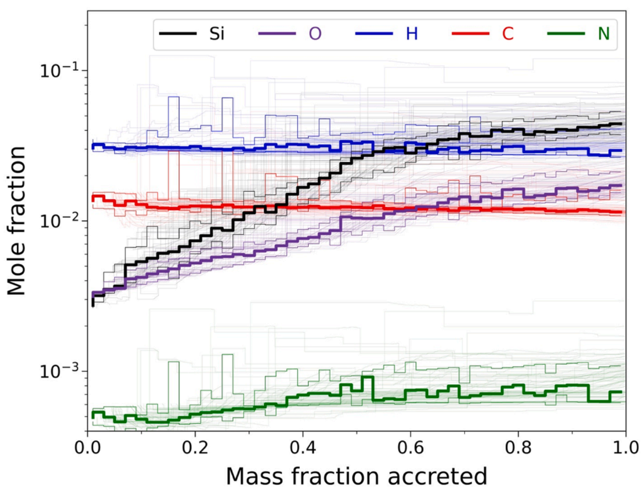

Fig. 6. Concentration of light elements in the core throughout accretion of Earth analogs using the metal–silicate partitioning of N from Jackson et al. (2021). Bold lines are medians and semi-bold lines are 10th and 90th percentiles of all Earth analogs. Thin lines are evolutions of individual Earth analogs. At the end of accretion, Earth analog cores contain $2.4^{+0.6}_{-0.5}$ wt% Si, $0.5^{+0.2}_{-0.1}$ wt% O, $0.06^{+0.03}_{-0.01}$ wt% H, $0.25^{+0.20}_{-0.04}$ wt% C, and $0.03^{+0.01}_{-0.01}$ wt% N. Si and O concentrations in the core increase as pressures and temperatures of equilibration increase, whereas concentrations of light elements remain relatively constant due to the siderophile nature of H, C, and N.

4. Discussion

4.1. Magma ocean redox

Magma oceans become more oxidized throughout accretion due to core formation (Rubie et al., 2011). However, magma ocean surfaces remain below the iron-wüstite buffer, resulting in CO-rich atmospheres throughout accretion. Our results rely on the abundance of Fe^{3+} in equilibrium with metal alloy from the molecular dynamics study of Deng et al. (2020), which predicts $Fe^{3+}/Fe_{tot} < 0.1$ (Fig. 3). These results conflict with experimental studies that indicate that Fe^{3+}/Fe_{tot} could increase dramatically with pressure, reaching values >0.35 (Armstrong et al., 2019; Kuwahara et al., 2023). However, subsequent crystallization and evolution of Earth's mantle must be consistent with basalt source regions that match the present-day upper mantle Fe^{3+}/Fe_{tot} of 0.04 ± 0.02 (Hirschmann, 2022). The effects of magma ocean solidification should be limited due to the relative compatibility of Fe^{3+} in bridgmanite and by homogenization of the mantle by convection (Kuwahara and Nakada, 2023). Iron disproportionation and hydrogen escape could both oxidize the mantle over time (Catling et al., 2001; Frost et al., 2004; Wordsworth et al., 2018; Zahnle et al., 2013). In contrast, late accretion may deliver metallic iron that reduces the mantle (Itcovitz et al., 2022; Zahnle et al., 2020), though it is unlikely that this mechanism is sufficient to reduce the mantle from the very oxidized values proposed by Kuwahara et al. (2023) (Hirschmann, 2023). We therefore favor the reduced case, but note that oxidized magma oceans would promote comparatively greater H and N loss relative (Supplementary Text S4). Future work on the redox evolution of magma oceans and Earth's mantle over time will be instrumental in constraining the distribution of volatile elements during Earth's formation.

4.2. Magma ocean crystallization

The distribution of volatiles between mantle and atmosphere after magma ocean crystallization determines the subsequent evolution and cycling between the two reservoirs. At the end of accretion, but before magma ocean crystallization, <<1% H, ~92% C, and 37–53% N of BSE (mantle + atmosphere) H, C, and N are in the atmosphere. These values contrast with the ~57% H, ~19% C, and ~58% N estimated to be on the surface and in the atmosphere today (Hirschmann, 2018). Compared to C, H and N are inefficiently recycled between the mantle and the surface over geologic timescales, suggesting that Earth's present-day surface H and N reservoirs were established early, shortly after magma ocean solidification (Hirschmann, 2018).

During crystallization of magma oceans, oxidation of the residual liquid could promote oxidation of atmospheres in equilibrium with the magma ocean, although the extent to which the residual liquid is oxidized depends on the partitioning of Fe^{3+} into bridgmanite (Boujibar et al., 2016; Kuwahara and Nakada, 2023). Oxidation and outgassing of some of the magma ocean's N could provide N from the mantle to the surface without requiring significant subsequent interior–atmosphere N exchange. For H, if magma ocean crystallization releases a maximum of 30% H (Bower et al., 2022; Miyazaki and Korenaga, 2022), outgassing of 1 ocean mass would require a total BSE H budget of >3.3 ocean masses. Smaller total H would require additional mantle degassing early in Earth's history (Médard and Grove, 2006) or late delivery of H that contributes to Earth's surface H (e.g., Wang and Becker, 2013). The strong temperature dependence of C solubility in silicate melts would lead to precipitation of diamond or graphite within the cooling magma ocean, which could incorporate C that was originally in the atmosphere into the mantle (Armstrong et al., 2019; Hirschmann, 2012; Keppler and Golabek, 2019; Sossi et al., 2020). Future work on the distribution of volatile elements during magma ocean crystallization will clarify the distribution of H, C, and N between Earth's mantle and atmosphere in the early Earth.

4.3. Additional model limitations

Our model provides constraints on the distributions of H, C, and N during Earth's formation by combining astrophysical *N*-body simulations with interior–atmosphere chemistry and atmosphere erosion. However, there are limitations within the scaling laws and parameterizations we apply that link these different processes together. Below, we outline additional assumptions that could affect our model results. Outputs of all model runs are provided in Supplementary Data.

We consider variations in individual parameters, including k_{core_emb}, impactor fO_2, the pressures and temperatures of metal–silicate equilibration, inner:outer Solar System volatile concentration ratio, and initial H:C:N volatile ratios (Supplementary Text S5). Of the free parameters in our model, k_{core_emb} is the most influential. Even though the abundances of H, C, and N in Earth analogs remain consistent with present-day BSE estimates for all values of k_{core_emb} (Fig. S8), complete equilibration ($k_{core\_emb} = 1$) decreases the fraction of C in Earth analog cores from ~63% to ~34% and increases C loss due to atmosphere erosion from ~26% to ~47% (Fig. S8). This is because increasing k_{core_emb} prevents the erosion of C by sequestering more C in the core. Increasing k_{core_emb} also increases the oxidizing effect of dissolving Si into the core, therefore oxidizing Earth analog mantles. Altering k_{core_emb} independently is consequently inconsistent with Earth's mantle FeO and trace element (Ni, Co, V, Cr, etc.) concentrations because it increases or decreases the abundance of metal that can sequester siderophile elements (Fischer et al., 2017). While the set of parameters we choose is non-unique, we conclude that adjusting parameters to match Earth's mantle composition will likely yield similar distributions of H, C, and N. For example, for a higher value of k_{core_emb}, decreasing the fO_2 of initial bodies will decrease C loss, negating the effects of changing k_{core_emb}.

We also vary the initial concentrations of H, C, and N at the beginning of *N*-body simulations. Changing only initial concentrations while keeping the inner:outer Solar System ratio of initial H, C, and N constant has very little effect on the proportion of H, C, and N in each reservoir, but affects the BSE abundances of each element (Fig. S8). Only C loss is noticeably affected, where using the smallest initial concentration consistent with the BSE's C content increases the proportion of C lost due to atmosphere erosion by ~5%. The effects of varying other parameters individually are discussed in Supplementary Text S5.

Magma oceans are assumed to crystallize before subsequent embryo impacts and are assumed to do so in our model (e.g., Nikolaou et al., 2019). However, we do not explicitly account for compositional effects of magma ocean crystallization, instead, holding mantle and atmosphere abundances of H, C, and N constant between impacts. Magma ocean crystallization could influence the interior–atmosphere distribution of H, C, and N by outgassing volatiles from the mantle to the atmosphere, potentially increasing the availability of each element to be eroded by subsequent impacts (Fig. S9). We have run additional models to assess the effects of magma ocean outgassing, in which a fixed fraction of the mantle's volatiles is outgassed and added to the atmosphere between embryo impacts. The distribution of H is most affected by outgassing between impacts because of the high solubility of H in magma oceans, increasing the fraction of H in the core from ~69% to ~91% when all volatiles are outgassed. However, recent studies of magma ocean crystallization that incorporate the trapping of volatiles in interstitial melts suggest that H could be efficiently retained in crystallized mantles (<30% outgassed), limiting the effects of outgassing on the distribution of H (Bower et al., 2022; Hier-Majumder and Hirschmann, 2017; Miyazaki and Korenaga, 2022).

It is possible that H_2/He atmospheres existed on initial planetary embryos, but these low mean molecular mass atmospheres are efficiently lost following impacts (Biersteker and Schlichting, 2021). The reaction of nebular H_2 with silicate or iron in embryos could increase the abundance of H relative to C and N and would result in non-chondritic H abundances (Horn et al., 2023; Young et al., 2023). However, the efficient storage of H in Earth analog interiors means that this additional H would most likely be stored in Earth's core, increasing the abundances of H in the core proposed in Section 3.3. H escape could alter the redox evolution of Earth analogs and further oxidize magma oceans (Catling et al., 2001; Wordsworth et al., 2018; Zahnle et al., 2013), but we do not consider hydrodynamic escape of volatile elements, as H escape is inefficient in high mean molecular mass and H-poor atmospheres (Biersteker and Schlichting, 2019).

There are also assumptions involved in our prescription of atmosphere erosion. Altering the minimum and maximum impactor size or increasing the differential power law index will change the impactor size distribution and therefore slightly modify the efficiency of planetesimals in eroding existing atmospheres (Supplementary Data). The scaling law for embryo erosion from Kegerreis et al. (2020) is based on loss of hydrogen–helium atmospheres. Erosion of higher mean molecular weight atmospheres would likely be less efficient, making our loss estimates upper bounds. Furthermore, atmosphere loss may be more efficient early in Earth's accretion when the proto-Earth had a smaller escape parameter (Sossi et al., 2022). The BSE's present-day volatile budget is therefore likely more representative of later-accreted material, as volatile loss was less efficient later in Earth's accretion, in addition to the more efficient sequestration of earlier-accreted volatiles in Earth's core (Dauphas, 2017).

5. Conclusions

We explore the effects of core formation and magma ocean redox on the distribution of H, C, and N during Earth's formation to determine the evolution of Earth's earliest atmosphere. Our model predicts that Earth had a CO-dominated atmosphere throughout accretion. This C-dominated atmosphere results in the preferential erosion of C (~18–45% is lost) relative to H and N, but significant N (~12–23%) can be lost if N is not strongly siderophile at high pressures and temperatures. Matching the BSE's C and H budgets requires volatile abundances in accreting materials to be depleted by ~1–2 orders of magnitude relative CI chondrite concentrations, on average, consistent with early volatile depletion on planetesimals and embryos. Volatile depletion on precursors is responsible for >92% of the BSE's volatile depletion relative to chondrites. Core formation and atmosphere erosion make up the remaining <8% of the BSE's volatile depletion but are both still crucial in setting the BSE's C/N ratio. The core is the major reservoir of H, C, and N in the Earth, making up ~57–75%, ~54%–98%, and ~69%–99.9% of the bulk Earth's budgets of these elements, respectively. Simulations that form Earth analogs with larger contributions of outer Solar System material, such as Classical and Grand Tack simulations, result in Earth analogs with higher total volatile concentrations and that lose a larger fraction of their accreted volatiles due to atmosphere erosion. Core formation alone can match or exceed the BSE's superchondritic C/N ratio if N is sufficiently siderophile at higher pressures and temperatures. If N is not sufficiently siderophile at high pressures and temperatures, however, the BSE's processes on precursor bodies must be responsible for elevating the BSE's C/N ratio. Future work on the redox states of magma oceans and the metal–silicate partitioning behavior of N will help to elucidate the fate of Earth's accreted volatile elements.

CRediT authorship contribution statement

Jesse T. Gu: Writing – review & editing, Writing – original draft, Methodology, Investigation. **Bo Peng:** Writing – review & editing, Writing – original draft, Methodology, Investigation. **Xuan Ji:** Writing – review & editing, Writing – original draft, Methodology, Investigation. **Jisheng Zhang:** Writing – review & editing, Methodology, Investigation. **Hong Yang:** Writing – review & editing, Methodology, Investigation. **Susana Hoyos:** Writing – review & editing, Project administration, Methodology, Investigation. **Marc M. Hirschmann:** Writing – review & editing, Supervision. **Edwin S. Kite:** Writing – review & editing, Supervision. **Rebecca A. Fischer:** Writing – review & editing, Supervision.

Declaration of competing interest

The authors declare that they have no known competing financial interests or personal relationships that could have appeared to influence the work reported in this paper.

Data availability

Data will be made available on request.

Acknowledgments

The authors thank the editor, James Badro, for handling of our manuscript, as well as Paolo Sossi and an anonymous reviewer for their helpful suggestions. This work originated from and benefited greatly from lectures and discussions at the CIDER 2022 Summer Program, which was funded by the NSF CSEDI Program (EAR-1903727). We would like to thank H. Schlichting, R. Pierrehumbert, J. Li, and J. Dong for helpful discussions and M. Clement, S. Jacobson, D. O'Brien, and S. Raymond for providing outputs of *N*-body simulations. This work was supported in part by an NSF Graduate Research Fellowship (DGE1745303) to J.T. Gu. R.A. Fischer and J.T. Gu were supported by a NASA Emerging Worlds grant (80NSSC21K0388) and an NSF CSEDI grant (EAR-2054912). M.M. Hirschmann's contributions were supported by NSF grant EAR-2016215 and NASA grant 80NSSC19K0959.

Supplementary materials

Supplementary material associated with this article can be found, in the online version, at doi:10.1016/j.epsl.2024.118618.

References

Abe, Y., Matsui, T., 1986. Early evolution of the Earth: accretion, atmosphere formation, and thermal history. J. Geophys. Res. 91 https://doi.org/10.1029/jb091ib13p0e291.

Abramov, O., Wong, S.M., Kring, D.A., 2012. Differential melt scaling for oblique impacts on terrestrial planets. Icarus 218, 906–916. https://doi.org/10.1016/j.icarus.2011.12.022.

Albarède, F., 2009. Volatile accretion history of the terrestrial planets and dynamic implications. Nature. https://doi.org/10.1038/nature08477.

Andrault, D., Bolfan-Casanova, N., Nigro, G.Lo, Bouhifd, M.A., Garbarino, G., Mezouar, M., 2011. Solidus and liquidus profiles of chondritic mantle: implication for melting of the Earth across its history. Earth. Planet. Sci. Lett. https://doi.org/10.1016/j.epsl.2011.02.006.

Armstrong, K., Frost, D.J., McCammon, C.A., Rubie, D.C., Ballaran, T.B., 2019. Deep magma ocean formation set the oxidation state of Earth's mantle. Science (1979) 365 (1979). https://doi.org/10.1126/science.aax8376.

Bergin, E.A., Blake, G.A., Ciesla, F., Hirschmann, M.M., Li, J., 2015. Tracing the ingredients for a habitable earth from interstellar space through planet formation. Proc. Natl. Acad. Sci. u S. a 112. https://doi.org/10.1073/pnas.1500954112.

Biersteker, J.B., Schlichting, H.E., 2021. Losing oceans: the effects of composition on the thermal component of impact-driven atmospheric loss. Mon. Not. R. Astron. Soc. 501, 587–595. https://doi.org/10.1093/mnras/staa3614.

Biersteker, J.B., Schlichting, H.E., 2019. Atmospheric mass-loss due to giant impacts: the importance of the thermal component for hydrogen-helium envelopes. Mon. Not. R. Astron. Soc. 485, 4454–4463. https://doi.org/10.1093/mnras/stz738.

Blanchard, I., Rubie, D.C., Jennings, E.S., Franchi, I.A., Zhao, X., Petitgirard, S., Miyajima, N., Jacobson, S.A., Morbidelli, A., 2022. The metal–silicate partitioning of carbon during Earth's accretion and its distribution in the early solar system. Earth. Planet. Sci. Lett. 580 https://doi.org/10.1016/j.epsl.2022.117374.

Boujibar, A., Bolfan-Casanova, N., Andrault, D., Ali Bouhifd, M., Trcera, N., 2016. Incorporation of Fe2+ and Fe3+ in bridgmanite during magma ocean crystallization. Am. Mineral. 101 https://doi.org/10.2138/am-2016-5561.

Bower, D.J., Hakim, K., Sossi, P.A., Sanan, P., 2022. Retention of water in terrestrial magma oceans and carbon-rich early atmospheres. Planet. Sci. J. 3 https://doi.org/10.3847/PSJ/ac5fb1.

Bower, D.J., Kitzmann, D., Wolf, A.S., Sanan, P., Dorn, C., Oza, A.V., 2019. Linking the evolution of terrestrial interiors and an early outgassed atmosphere to astrophysical observations. Astron. Astrophys. 631 https://doi.org/10.1051/0004-6361/201935710.

Brennan, M.C., Fischer, R.A., Nimmo, F., O'Brien, D.P., 2022. Timing of Martian core formation from models of Hf–W evolution coupled with N-body simulations. Geochim. Cosmochim. Acta 316, 295–308. https://doi.org/10.1016/j.gca.2021.09.022.

Broadley, M.W., Bekaert, D.v., Piani, L., Füri, E., Marty, B., 2022. Origin of life-forming volatile elements in the inner Solar System. Nature. https://doi.org/10.1038/s41586-022-05276-x.

Catling, D.C., Zahnle, K.J., McKay, C.P., 2001. Biogenic methane, hydrogen escape, and the irreversible oxidation of early earth. Science (1979) 293 (1979). https://doi.org/10.1126/science.1061976.

Chen, H., Jacobson, S.A., 2022. Impact induced atmosphere-mantle exchange sets the volatile elemental ratios on primitive Earths. Earth. Planet. Sci. Lett. 594 https://doi.org/10.1016/j.epsl.2022.117741.

Clement, M.S., Kaib, N.A., Raymond, S.N., Chambers, J.E., 2021. The early instability scenario: mars' mass explained by Jupiter's orbit. Icarus 367, 114585. https://doi.org/10.1016/j.icarus.2021.114585.

Dasgupta, R., Falksen, E., Pal, A., Sun, C., 2022. The fate of nitrogen during parent body partial melting and accretion of the inner solar system bodies at reducing conditions. Geochim. Cosmochim. Acta 336, 291–307. https://doi.org/10.1016/j.gca.2022.09.012.

Dauphas, N., 2017. The isotopic nature of the Earth's accreting material through time. Nature 541, 521–524. https://doi.org/10.1038/nature20830.

Deng, J., Du, Z., Karki, B.B., Ghosh, D.B., Lee, K.K.M., 2020. A magma ocean origin to divergent redox evolutions of rocky planetary bodies and early atmospheres. Nat. Commun. 11 https://doi.org/10.1038/s41467-020-15757-0.

Fischer, R.A., Campbell, A.J., Ciesla, F.J., 2017. Sensitivities of Earth's core and mantle compositions to accretion and differentiation processes. Earth. Planet. Sci. Lett. 458, 252–262. https://doi.org/10.1016/j.epsl.2016.10.025.

Fischer, R.A., Cottrell, E., Hauri, E., Lee, K.K.M., Le Voyer, M., 2020. The carbon content of Earth and its core. Proc. Natl. Acad. Sci. 117, 8743–8749. https://doi.org/10.1073/pnas.1919930117.

Fischer, R.A., Nakajima, Y., Campbell, A.J., Frost, D.J., Harries, D., Langenhorst, F., Miyajima, N., Pollok, K., Rubie, D.C., 2015. High pressure metal–silicate partitioning of Ni, Co, V, Cr, Si, and O. Geochim. Cosmochim. Acta 167, 177–194. https://doi.org/10.1016/j.gca.2015.06.026.

Fleck, J.R., Rains, C.L., Weeraratne, D.S., Nguyen, C.T., Brand, D.M., Klein, S.M., McGehee, J.M., Rincon, J.M., Martinez, C., Olson, P.L., 2018. Iron diapirs entrain silicates to the core and initiate thermochemical plumes. Nat. Commun. 9, 1–12. https://doi.org/10.1038/s41467-017-02503-2.

Frost, D.J., Liebske, C., Langenhorst, F., McCammon, C.A., Trønnes, R.G., Rubie, D.C., 2004. Experimental evidence for the existence of iron-rich metal in the Earth's lower mantle. Nature 428. https://doi.org/10.1038/nature02413.

Gaillard, F., Bernadou, F., Roskosz, M., Bouhifd, M.A., Marrocchi, Y., Iacono-Marziano, G., Moreira, M., Scaillet, B., Rogerie, G., 2022. Redox controls during magma ocean degassing. Earth. Planet. Sci. Lett. 577 https://doi.org/10.1016/j.epsl.2021.117255.

Genda, H., Abe, Y., 2005. Enhanced atmospheric loss on protoplanets at the giant impact phase in the presence of oceans. Nature 433. https://doi.org/10.1038/nature03360.

Grewal, D.S., Asimow, P.D., 2023. Origin of the superchondritic carbon/nitrogen ratio of the bulk silicate Earth – an outlook from iron meteorites. Geochim. Cosmochim. Acta 344, 146–159. https://doi.org/10.1016/j.gca.2023.01.012.

Gu, J.T., Fischer, R.A., Brennan, M.C., Clement, M.S., Jacobson, S.A., Kaib, N.A., O'Brien, D.P., Raymond, S.N., 2023. Comparisons of the core and mantle compositions of earth analogs from different terrestrial planet formation scenarios. Icarus 394. https://doi.org/10.1016/j.icarus.2023.115425.

Halliday, A.N., 2013. The origins of volatiles in the terrestrial planets. Geochim. Cosmochim. Acta 105. https://doi.org/10.1016/j.gca.2012.11.015.

Hier-Majumder, S., Hirschmann, M.M., 2017. The origin of volatiles in the Earth's mantle. Geochem., Geophys., Geosyst. 18, 3078–3092. https://doi.org/10.1002/2017GC006937.

Hirschmann, M.M., 2023. The deep Earth oxygen cycle: mass balance considerations on the origin and evolution of mantle and surface oxidative reservoirs. Earth. Planet. Sci. Lett. 619 https://doi.org/10.1016/j.epsl.2023.118311.

Hirschmann, M.M., 2022. Magma oceans, iron and chromium redox, and the origin of comparatively oxidized planetary mantles. Geochim. Cosmochim. Acta 328, 221–241. https://doi.org/10.1016/j.gca.2022.04.005.

Hirschmann, M.M., 2021. Iron-wüstite revisited: a revised calibration accounting for variable stoichiometry and the effects of pressure. Geochim. Cosmochim. Acta 313, 74–84. https://doi.org/10.1016/j.gca.2021.08.039.

Hirschmann, M.M., 2018. Comparative deep Earth volatile cycles: the case for C recycling from exosphere/mantle fractionation of major (H2O, C, N) volatiles and from H2O/Ce, CO2/Ba, and CO2/Nb exosphere ratios. Earth. Planet. Sci. Lett. 502 https://doi.org/10.1016/j.epsl.2018.08.023.

Hirschmann, M.M., 2016. Constraints on the early delivery and fractionation of Earth's major volatiles from C/H, C/N, and C/S ratios. Am. Mineral. 101, 540–553. https://doi.org/10.2138/am-2016-5452.

Hirschmann, M.M., 2012. Magma ocean influence on early atmosphere mass and composition. Earth. Planet. Sci. Lett. 341–344, 48–57. https://doi.org/10.1016/j.epsl.2012.06.015.

Hirschmann, M.M., Bergin, E.A., Blake, G.A., Ciesla, F.J., Li, J., 2021. Early volatile depletion on planetesimals inferred from C–S systematics of iron meteorite parent bodies. Proc. Natl. Acad. Sci. u S. a 118. https://doi.org/10.1073/pnas.2026779118.

Horn, H.W., Prakapenka, V., Chariton, S., Speziale, S., Shim, S.-H., 2023. Reaction between hydrogen and ferrous/ferric oxides at high pressures and high temperatures—implications for sub-neptunes and super-earths. Planet. Sci. J. 4, 30. https://doi.org/10.3847/psj/acab03.

Itcovitz, J.P., Rae, A.S.P., Citron, R.I., Stewart, S.T., Sinclair, C.A., Rimmer, P.B., Shorttle, O., 2022. Reduced atmospheres of post-impact worlds: the early earth. Planet. Sci. J. 3 https://doi.org/10.3847/PSJ/ac67a9.

Jackson, C.R.M., Cottrell, E., Du, Z., Bennett, N.R., Fei, Y., 2021. High pressure redistribution of nitrogen and sulfur during planetary stratification. Geochem. Perspect. Lett. 18, 37–42. https://doi.org/10.7185/geochemlet.2122.

Jacobson, S.A., Morbidelli, A., 2014. Lunar and terrestrial planet formation in the Grand Tack scenario. Philos. Trans. R. Soc. A: Math., Phys. Eng. Sci. https://doi.org/10.1098/rsta.2013.0174.

Johansen, A., Ronnet, T., Bizzarro, M., Schiller, M., Lambrechts, M., Nordlund, A., Lammer, H., 2021. A pebble accretion model for the formation of the terrestrial planets in the solar system. Sci. Adv. 7 https://doi.org/10.1126/sciadv.abc0444.

Kegerreis, J.A., Eke, V.R., Catling, D.C., Massey, R.J., Teodoro, L.F.A., Zahnle, K.J., 2020. Atmospheric erosion by giant impacts onto terrestrial planets: a scaling law for any speed, angle, mass, and density. Astrophys. J. 901, L31. https://doi.org/10.3847/2041-8213/abb5fb.

Kendall, J.D., Melosh, H.J., 2016. Differentiated planetesimal impacts into a terrestrial magma ocean: fate of the iron core. Earth. Planet. Sci. Lett. 448, 24–33. https://doi.org/10.1016/j.epsl.2016.05.012.

Keppler, H., Golabek, G., 2019. Graphite floatation on a magma ocean and the fate of carbon during core formation. Geochem. Perspect. Lett. 11 https://doi.org/10.7185/geochemlet.1918.

Kuwahara, H., Nakada, R., 2023. Partitioning of Fe2+ and Fe3+ between bridgmanite and silicate melt: implications for redox evolution of the Earth's mantle. Earth. Planet. Sci. Lett. 615, 118197 https://doi.org/10.1016/j.epsl.2023.118197.

Kuwahara, H., Nakada, R., Kadoya, S., Yoshino, T., Irifune, T., 2023. Hadean mantle oxidation inferred from melting of peridotite under lower-mantle conditions. Nat. Geosci. https://doi.org/10.1038/s41561-023-01169-4.

Li, J., Bergin, E.A., Blake, G.A., Ciesla, F.J., Hirschmann, M.M., 2021. Earth's carbon deficit caused by early loss through irreversible sublimation. Sci. Adv.

Li, J., Chen, B., Mookherjee, M., Morard, G., 2019. Deep Carbon. Cambridge University Press. https://doi.org/10.1017/9781108677950.

Li, Y., Wiedenbeck, M., Monteleone, B., Dasgupta, R., Costin, G., Gao, Z., Lu, W., 2023. Nitrogen and carbon fractionation in planetary magma oceans and origin of the superchondritic C/N ratio in the bulk silicate Earth. Earth. Planet. Sci. Lett. 605 https://doi.org/10.1016/j.epsl.2023.118032.

Lichtenberg, T., Bower, D.J., Hammond, M., Boukrouche, R., Sanan, P., Tsai, S.M., Pierrehumbert, R.T., 2021. Vertically resolved magma ocean–protoatmosphere evolution: H2, H2O, CO2, CH4, CO, O2, and N2 as primary absorbers. J. Geophys. Res. Planets. 126 https://doi.org/10.1029/2020JE006711.

Lichtenberg, T., Golabek, G.J., Burn, R., Meyer, M.R., Alibert, Y., Gerya, T.V., Mordasini, C., 2019. A water budget dichotomy of rocky protoplanets from 26 Al-heating. Nat. Astron. https://doi.org/10.1038/s41550-018-0688-5.

Linstorm, P., 1998. NIST chemistry WebBook, NIST standard reference database number 69. J. Phys. Chem. Ref. Data, Monograph 9, 1–1951.

Marchi, S., Canup, R.M., Walker, R.J., 2018. Heterogeneous delivery of silicate and metal to the Earth by large planetesimals. Nat. Geosci. 11, 77–81. https://doi.org/10.1038/s41561-017-0022-3.

Marty, B., 2012. The origins and concentrations of water, carbon, nitrogen and noble gases on Earth. Earth. Planet. Sci. Lett. 313–314. https://doi.org/10.1016/j.epsl.2011.10.040.

Marty, B., Almayrac, M., Barry, P.H., Bekaert, D.V., Broadley, M.W., Byrne, D.J., Ballentine, C.J., Caracausi, A., 2020. An evaluation of the C/N ratio of the mantle from natural CO2-rich gas analysis: geochemical and cosmochemical implications. Earth. Planet. Sci. Lett. 551 https://doi.org/10.1016/j.epsl.2020.116574.

Marty, B., Zimmermann, L., 1999. Volatiles (He, C, N, Ar) in mid-ocean ridge basalts: assesment of shallow-level fractionation and characterization of source composition. Geochim. Cosmochim. Acta 63. https://doi.org/10.1016/S0016-7037(99)00169-6.

McDonough, W.F.F., Sun, S.-s.s., 1995. The composition of the Earth. Chem Geol 120, 223–253. https://doi.org/10.1016/0009-2541(94)00140-4.

Médard, E., Grove, T.L., 2006. Early hydrous melting and degassing of the Martian interior. J. Geophys. Res. Planets. 111 https://doi.org/10.1029/2006JE002742.

Miyazaki, Y., Korenaga, J., 2022. Inefficient water degassing inhibits ocean formation on rocky planets: an insight from self-consistent mantle degassing models. Astrobiology. https://doi.org/10.1089/ast.2021.0126.

Nakajima, M., Golabek, G.J., Wünnemann, K., Rubie, D.C., Burger, C., Melosh, H.J., Jacobson, S.A., Manske, L., Hull, S.D., 2021. Scaling laws for the geometry of an impact-induced magma ocean. Earth. Planet. Sci. Lett. 568, 116983 https://doi.org/10.1016/j.epsl.2021.116983.

Newcombe, M.E., Nielsen, S.G., Peterson, L.D., Wang, J., Alexander, C.M.O.D., Sarafian, A.R., Shimizu, K., Nittler, L.R., Irving, A.J., 2023. Degassing of early-formed planetesimals restricted water delivery to Earth. Nature. https://doi.org/10.1038/s41586-023-05721-5.

Nikolaou, A., Katyal, N., Tosi, N., Godolt, M., Grenfell, J.L., Rauer, H., 2019. What Factors Affect the Duration and Outgassing of the Terrestrial Magma Ocean? Astrophys. J. 875, 11. https://doi.org/10.3847/1538-4357/ab08ed.

O'Brien, D.P., Morbidelli, A., Levison, H.F., 2006. Terrestrial planet formation with strong dynamical friction. Icarus 184, 39–58. https://doi.org/10.1016/j.icarus.2006.04.005.

Okuchi, T., 1997. Hydrogen partitioning into molten iron at high pressure: implications for earth's core. Science (1979) (1979). https://doi.org/10.1126/science.278.5344.1781.

Palme, H., O'Neill, H., 2014. Cosmochemical Estimates of Mantle Composition, 2nd ed, Treatise on Geochemistry: Second Edition. Elsevier Ltd. https://doi.org/10.1016/B978-0-08-095975-7.00201-1.

Raymond, S.N., Izidoro, A., 2017. The empty primordial asteroid belt. Sci. Adv. 3 https://doi.org/10.1126/sciadv.1701138.

Raymond, S.N., O'Brien, D.P., Morbidelli, A., Kaib, N.A., 2009. Building the terrestrial planets: constrained accretion in the inner Solar System. Icarus 203, 644–662. https://doi.org/10.1016/j.icarus.2009.05.016.

Robie, R.A., Hemingway, B.S., 1995. Thermodynamic properties of minerals and related substances at 298.15K and 1bar (10ˆ5 Pa) pressure and at higher temperatures. Bulletin. https://doi.org/10.3133/b2131.

Rubie, D.C., Frost, D.J., Mann, U., Asahara, Y., Nimmo, F., Tsuno, K., Kegler, P., Holzheid, A., Palme, H., 2011. Heterogeneous accretion, composition and core–mantle differentiation of the Earth. Earth. Planet. Sci. Lett. 301, 31–42. https://doi.org/10.1016/j.epsl.2010.11.030.

Rubie, D.C., Jacobson, S.A., Morbidelli, A., O'Brien, D.P., Young, E.D., de Vries, J., Nimmo, F., Palme, H., Frost, D.J., 2015. Accretion and differentiation of the terrestrial planets with implications for the compositions of early-formed Solar System bodies and accretion of water. Icarus 248, 89–108. https://doi.org/10.1016/j.icarus.2014.10.015.

Sakuraba, H., Kurokawa, H., Genda, H., Ohta, K., 2021. Numerous chondritic impactors and oxidized magma ocean set Earth's volatile depletion. Sci. Rep. 11 https://doi.org/10.1038/s41598-021-99240-w.

Salvador, A., Samuel, H., 2023. Convective outgassing efficiency in planetary magma oceans: insights from computational fluid dynamics. Icarus 390. https://doi.org/10.1016/j.icarus.2022.115265.

Schlichting, H.E., Sari, R., Yalinewich, A., 2015. Atmospheric mass loss during planet formation: the importance of planetesimal impacts. Icarus 247, 81–94. https://doi.org/10.1016/j.icarus.2014.09.053.

Schönbächler, M., Carlson, R.W., Horan, M.F., Mock, T.D., Hauri, E.H., 2010. Heterogeneous accretion and the moderately volatile element budget of earth. Science (1979) 328 (1979). https://doi.org/10.1126/science.1186239.

Shi, L., Lu, W., Kagoshima, T., Sano, Y., Gao, Z., Du, Z., Liu, Y., Fei, Y., Li, Y., 2022. Nitrogen isotope evidence for Earth's heterogeneous accretion of volatiles. Nat. Commun. 13 https://doi.org/10.1038/s41467-022-32516-5.

Shuvalov, V., 2009. Atmospheric erosion induced by oblique impacts. Meteorit. Planet. Sci. 44, 1095–1105. https://doi.org/10.1111/j.1945-5100.2009.tb01209.x.

Shuvalov, V., Kührt, E., De Niem, D., Wünnemann, K., 2014. Impact induced erosion of hot and dense atmospheres. Planet Space Sci 98, 120–127. https://doi.org/10.1016/j.pss.2013.08.018.

Sinclair, C.A., Wyatt, M.C., 2022. The role of impacts on the atmospheres on the moons of outer giants. Mon. Not. R. Astron. Soc. 509 https://doi.org/10.1093/mnras/stab3026.

Sossi, P.A., Burnham, A.D., Badro, J., Lanzirotti, A., Newville, M., StC, H.O., 2020. Redox state of Earth's magma ocean and its Venus-like early atmosphere. Sci. Adv.

Sossi, P.A., Stotz, I.L., Jacobson, S.A., Morbidelli, A., O'Neill, H.S.C., 2022. Stochastic accretion of the Earth. Nat. Astron. 6, 951–960. https://doi.org/10.1038/s41550-022-01702-2.

Tagawa, S., Sakamoto, N., Hirose, K., Yokoo, S., Hernlund, J., Ohishi, Y., Yurimoto, H., 2021. Experimental evidence for hydrogen incorporation into Earth's core. Nat. Commun. 12 https://doi.org/10.1038/s41467-021-22035-0.

Thomas, B., Samuel, H., Farnetani, C.G., Aubert, J., Chauvel, C., 2023. Mixing time of heterogeneities in a buoyancy-dominated magma ocean. https://doi.org/10.1093/gji/ggad452/7440027.

Thomas, C.W., Asimow, P.D., 2013. Direct shock compression experiments on premolten forsterite and progress toward a consistent high-pressure equation of state for CaO-MgO-Al 2O3-SiO2-FeO liquids. J. Geophys. Res. Solid. Earth. 118 https://doi.org/10.1002/jgrb.50374.

Tucker, J.M., Mukhopadhyay, S., 2014. Evidence for multiple magma ocean outgassing and atmospheric loss episodes from mantle noble gases. Earth. Planet. Sci. Lett. https://doi.org/10.1016/j.epsl.2014.02.050.

Vacher, L.G., Piani, L., Rigaudier, T., Thomassin, D., Florin, G., Piralla, M., Marrocchi, Y., 2020. Hydrogen in chondrites: influence of parent body alteration and atmospheric contamination on primordial components. Geochim. Cosmochim. Acta 281, 53–66. https://doi.org/10.1016/j.gca.2020.05.007.

Wang, Z., Becker, H., 2013. Ratios of S, Se and Te in the silicate Earth require a volatile-rich late veneer. Nature 499. https://doi.org/10.1038/nature12285.

Wasson, J.T., Kallemeyn, G.W., 1988. Compositions of chondrites. Philos. Trans. R. Soc. London. Ser. A, Math. Phys. Sci. 325, 535–544. https://doi.org/10.1098/rsta.1988.0066.

Wordsworth, R.D., Schaefer, L.K., Fischer, R.A., 2018. Redox evolution via gravitational differentiation on low-mass planets: implications for abiotic oxygen, water loss, and habitability. Astron. J. 155 https://doi.org/10.3847/1538-3881/aab608.

Young, E.D., Shahar, A., Schlichting, H.E., 2023. Earth shaped by primordial H2 atmospheres. Nature 616, 306–311. https://doi.org/10.1038/s41586-023-05823-0.

Zahnle, K.J., Catling, D.C., Claire, M.W., 2013. The rise of oxygen and the hydrogen hourglass. Chem. Geol. 362 https://doi.org/10.1016/j.chemgeo.2013.08.004.

Zahnle, K.J., Lupu, R., Catling, D.C., Wogan, N., 2020. Creation and evolution of impact-generated reduced atmospheres of early earth. Planet. Sci. J. 1 https://doi.org/10.3847/PSJ/ab7e2c.

Zhang, H.L., Hirschmann, M.M., Cottrell, E., Withers, A.C., 2017. Effect of pressure on Fe3+/ΣFe ratio in a mafic magma and consequences for magma ocean redox gradients. Geochim. Cosmochim. Acta 204, 83–103. https://doi.org/10.1016/j.gca.2017.01.023.